AIAA JOURNAL
Vol. 35, No. 11, November 1997

Interference Between a Cylindrical Bow Shock and a Plane Oblique Shock

V. Ya. Borovoy,* A. Yu. Chinilov,† V. N. Gusev,‡ and I. V. Struminskaya§
Central Aerohydrodynamics Institute (TsAGI), Zhukovsky 140160, Russia
and
J. Délery¶ and B. Chanetz**
ONERA, 92320 Châtillon, France

Hypersonic flows are prone to intense shock waves whose intersection, or interference, gives rise to a system of waves and slip surfaces that can have a large influence on the aerodynamics of a vehicle. It is convenient to distinguish six types of interference associated with very distinct flow structures, depending on the intensity and relative direction of the intersecting shock waves. Among these classes of interference, those of types III and IV are the origin of shear layers or supersonic jets whose impact on a nearby surface creates potentially destructive peaks of pressure and heat flux locally. Type III and IV interference and the corresponding heat transfer distributions were investigated experimentally. The model consisted of a cylindrically blunted plate and a wedge serving as an oblique shock generator. These experiments were carried out in a short-duration wind tunnel at Mach numbers 6 and 16 in air and at Mach number 6.6 in carbon dioxide. The Reynolds number based on the plate bluntness diameter was varied in the range from 2.2×10^4 to 1.6×10^6. The influence of the impinging shock location on the interference heat transfer was carefully investigated. Estimations of the maximum interference heat transfer rate, based on inviscid flow calculations and a boundary-layer approach, compare well with the data. The effect of the specific heat ratio on the interference flow was studied.

Nomenclature

D	= nozzle exit diameter
d	= cylinder diameter, $2r$
L	= wedge length
M_∞	= undisturbed flow Mach number
P_s	= stagnation pressure
P_0	= total pressure
q	= heat transfer rate
q_m	= peak heat transfer in the interference region
q_0	= stagnation point heat transfer on the cylinder alone
Re	= Reynolds number referenced to the cylinder diameter
X, Y	= horizontal and vertical distance between wedge and plate (see Fig. 2)
x_*	= shock coordinate characterizing the location of the impinging shock relative to the cylinder (defined in Fig. 2)
γ	= specific heat ratio
θ	= wedge angle
μ	= molecular viscosity
ρ	= density
σ	= direction of the velocity in shock polar representation
φ	= angular coordinate defined in Fig. 2
φ_m	= angular coordinate of peak heat flux

Presented as Paper 96-2046 at the AIAA 27th Fluid Dynamics Conference, New Orleans, LA, June 17–20, 1996; received Sept. 26, 1996; revision received June 24, 1997; accepted for publication June 25, 1997.

*Professor, Heat Protection Branch, Aerothermodynamics Division.
†Research Scientist, Computational Fluid Dynamics Branch, Aerothermodynamics Division.
‡Professor, Deputy Director.
§Leading Engineer, Heat Protection Branch, Aerothermodynamics Division.
¶Head, Fundamental Aerodynamics Branch, 29, avenue de la Division Leclerc. Member AIAA.
**Head, Hypersonic Research Group, 29, avenue de la Division Leclerc.

I. Introduction

ONE of the most challenging problems of gasdynamics is shock/shock interference. Even in an inviscid flow, shock interferences lead to complex combinations of shocks, expansion fans, slip surfaces, and jets. Additional complications are associated with the viscosity of the fluid and laminar–turbulent transition, as well as physical and chemical gas transformations. The study of shock wave interference is also of great interest for practical applications and is indispensable for understanding heat transfer mechanisms on a hypersonic vehicle surface.

Historically, the study of interference can be divided into two periods. During the first, investigations were mainly concerned with the flow over the leading edges of wings, tails, and pylons. The problem is represented by a plane shock wave impinging on a cylinder at some angle to its generatrices. One of the first investigations, published in 1967, revealed that heat transfer and pressure levels in the interference region are several times higher than on the cylinder alone (without impinging shock).[1] In 1968, Edney[2] performed an extensive experimental investigation of the phenomenon and defined six types of interference.

After the first period, workers were more concerned with hypersonic air intakes, in which the shocks produced by the compression ramps intersect the bow shock that forms ahead of the cowl (blunted to limit heat transfer). In the present paper, the situation is simulated in a two-dimensional flow by considering the intersection between a bow shock in front of a cylinder and a plane oblique shock parallel to the cylinder axis. Several papers present results of extensive experimental investigations at Mach numbers from 6 to 16, showing that heat transfer and pressure amplifications also take place for two-dimensional interference.[3–5] In certain articles, interference has been investigated numerically using the Navier–Stokes equations.[6–8] Although the computed pressure distributions compare well with the experimental data, large discrepancies in the heat transfer values are sometimes found.

To introduce the different interferences, we shall consider an oblique shock C_1 meeting the detached shock C_2, which forms ahead of a blunt obstacle. Let us suppose that C_1 is propagating from below. Edney,[2] by analyzing carefully conducted experiments, was able to identify six types, or patterns, of basic interferences, as is represented in Fig. 1. The shock C_2 is the bow shock ahead of

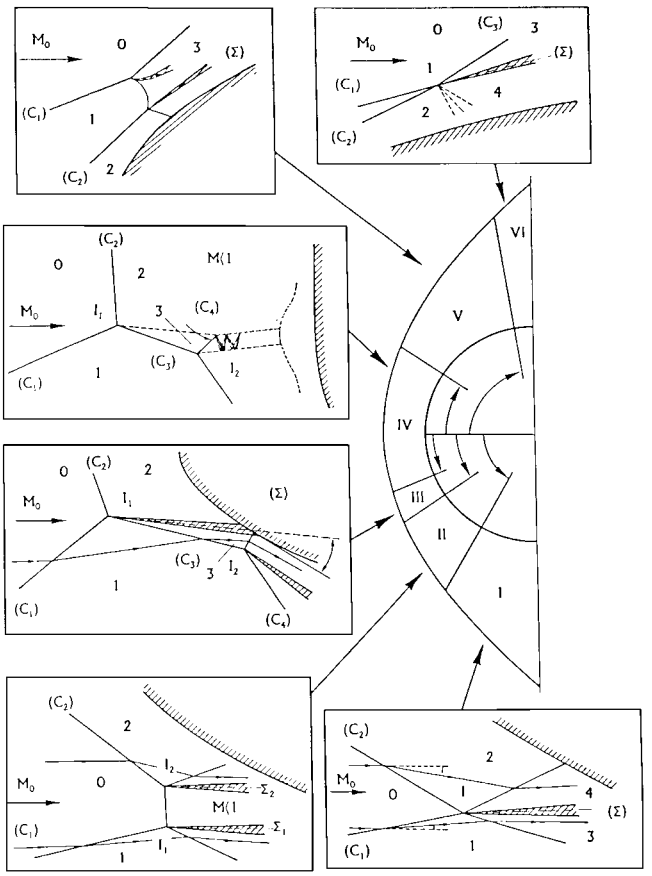

Fig. 1 Different shock/shock interference types.

a cylinder and the weak oblique shock C_1 meets the shock C_2 at different locations showing the following different types of interference.

1) When the incident shock C_1 crosses the bow shock C_2 underneath the lower sonic line, the situation corresponds to the intersection of two oblique shocks coming from opposite directions. Two situations occur downstream the meeting point: the first, called type I interference, characterized by the formation of two shocks C_3 and C_4 emanating from the meeting point and the second, called type II interference, in which two triple points are formed separated by a normal shock. Such a structure is called a Mach phenomenon.

2) When the oblique shock crosses the bow shock in the area where it is a strong shock, the two shocks have very different intensities, and a slip line results from this interference, separating a region above this line where the flow is subsonic, with low velocity, from a region underneath with supersonic flow and high velocity. When the reattachment of the slip line is possible on the obstacle, the situation is called type III interference. When it is impossible, the slip line is followed by a supersonic jet surrounded by a subsonic flow. When the supersonic jet impacts the cylinder, the situation corresponds to type IV interference. In some cases the supersonic jet is too curved, deflects upward, and grazes the cylinder surface. This situation is called, in this paper, type IVa interference.

3) When the oblique shock crosses the bow shock above the upper sonic line in a region where they are both weak oblique shocks of the same direction, two situations are observed. In the type V interference, the resulting field adopts a complex structure with two multiple points, akin to that associated with interference of type II, but this time a supersonic jet leaves from the upper multiple point, instead of a simple slip line. The type VI interference occurs when the shocks C_1 and C_2 cross far from the nose. In this situation the two shocks meet at the triple point from which a shock C_3, a slip line, and an expansion wave leave.

In the present work, an experimental study of shock/shock interference was performed in the Central Aerohydrodynamics Institute (TsAGI) UT-1 short-duration wind tunnel. This investigation focused on types III and IV interference, which results in the most severe increases of heat transfer rate. Nearly 120 interference patterns have been studied at Mach numbers $M_\infty = 6, 6.6$, and 16. The plane oblique shock was generated by wedges of angle θ ranging from 10 to 20 deg. The plate producing the bow shock wave was cylindrically blunted. The effects of the impinging shock location and Reynolds number on the heat transfer distribution were carefully studied. Also, experiments in a carbon dioxide flow were undertaken to simulate phenomena occurring in the air at high temperature.

II. Experimental Technique

A. TsAGI UT-1 Wind Tunnel

The experiments were performed in the short-duration UT-1 wind tunnel, which can be operated either as a Ludwieg tunnel or as a shock tunnel. In the Ludwieg tunnel arrangement, the high-pressure tube consists of two sections, each having a length of 6 m and an inner diameter of 70 mm. An external electrical heater can heat the working gas up to 800 K. The maximum pressure in the tube is 100×10^5 Pa if two sections are used and 200×10^5 Pa when one is used. The high-pressure tube is connected to the nozzle. There is a set of contoured nozzles for producing uniform flow at different Mach numbers. The gas flows from the nozzle into the test section, which is 1 m long and 0.5 m in diameter, and then expands into a vacuum vessel. After rupture of the double diaphragm arrangement, a quasi-steady flow exists in the test section before the arrival of the expansion waves reflected by the left end of the tube. The maximum stationary flow duration is about 40 ms if two tube sections are used and 20 ms if one is used. The gas pressure and temperature in the high-pressure tube were measured at the moment of the diaphragm rupture.

In the shock tunnel arrangement, the high-pressure section is filled with helium. After rupture of the diaphragm, the shock wave travels through the working gas and, after rupture of a second diaphragm, air expands through the nozzle to the test section. The duration of the steady flow is about 6 ms. The maximum pressure in the high-pressure section is 200×10^5 Pa. During the tests, the initial pressure in the high- and low-pressure sections and the pressure in front of the nozzle P_5 (practically equal to the total pressure P_0) are measured. The air total temperature, equal to the temperature T_5 downstream of the reflected shock, was determined using known relations along with real air thermodynamics.

The Mach number in the test section depends on the nozzle boundary-layer thickness and, consequently, on the total pressure and temperature. To evaluate the Mach number, the stagnation pressure was measured under the same conditions as in the model tests.

For this purpose, a stagnation pressure rake equipped with 7 or 11 probes was used. For flow visualization at $M_\infty = 6$ and 6.6, a direct shadowgraph method was used. In this case, its sensitivity appeared to be too high, which was manifested in an excessive image width of shock waves and a distortion of the model image. To provide adequate sensitivity, the direct shadowgraph method was improved by placing a lens in such a way that the recording plane, optically conjugated with the film plane, was introduced into the flow. For flow visualization at $M_\infty = 16$, at which the air density is very small, a knife edge was introduced into the optical system. A pulse lamp with a spark duration of 1 μs was used as a light source in both cases.

B. Model Arrangement

The experimental arrangement and the model definition are presented in Fig. 2. The model consists of a cylindrically blunted plate and a wedge generating a plane oblique shock wave. In some experiments, end plates were used to investigate the effect of model span on the flow structure and heat transfer. Many preliminary tests were performed to determine the maximum model dimensions: the plate thickness was 30 mm, its lateral span 150 mm, and the maximum wedge length in the flow direction 250 mm. The dimensions were limited by the inviscid flow core diameter. In addition, the model should not choke the wind tunnel. The model thickness was chosen to allow a large number of sensors on its front surface, providing the required spatial resolution to measure the heat flux distribution. The length of the wedges in the flow direction was large enough, so that the expansion waves emanating from their trailing edge did not affect the flow in the investigated interference region. To vary the impinging shock strength, different wedges were used with angles ranging from $\theta = 10$ to 20 deg.

Table 1 Flow parameters near wedge (air)

M	$Re \times 10^{-6}$	θ, deg	L, mm	M_1	β_{th}, deg	β_{exp}, deg
6	0.45	10	250	4.65	17.59	16.67
		15	200	3.99	22.67	22.05
		20	130	3.38	28.26	27.47
16	0.011	10	250	8.35	13.09	13.09
		15	200	6.11	18.87	19.57
		20	130	4.65	24.92	25.38

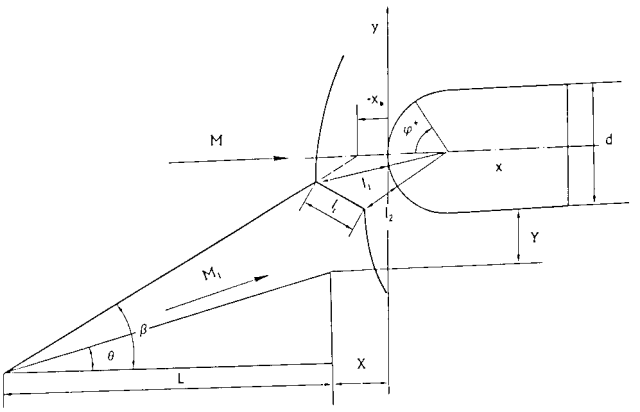

Fig. 2 Model definition.

Table 1 presents the geometric characteristics of the wedges and the calculated values of the inviscid flow parameters: wedge surface Mach number M_1, oblique shock wave β angle, and measured values of this angle, β_{exp}.

The blunted plate is mounted to a pylon and the wedge on a sliding element, so that the two can be moved along rails in the x direction. In addition, the wedge can be moved in the y direction. The distances set between the wedge and the plate were accurate to 0.1 mm. Plate 1 consists of two parts: a semicylindrical nose and a plane body, manufactured from stainless steel. The plate covers provide excess for the printed circuit inserts where the thermocouple wires are soldered.

C. Instrumentation

Most of the heat transfer measurements were performed by the thin wall technique. This method was implemented as follows. A 21-mm-wide foil strip was soldered to the cylindrical model surface in the vicinity of the plane of symmetry. Two plates were made, differing only by the thickness and material of the strip. In most experiments, the stainless-steel strip of 0.1 mm thickness was used. In the rest, another model with a nichrom strip of 0.2 mm thickness was used. The 0.1-mm thermocouple wires were soldered to the inner side of the foil at two sections located at 4 mm from the plane of symmetry. Near the solder point, the wires were rolled off with special rolls to a thickness of 0.03–0.04 mm. Because of the soldering technique, unconventional copel-stainless steel or copel-nichrom thermocouples were used. Considering both sections together, the thermocouples in the highest density region were spaced 1 deg or 0.26 mm apart (50 thermocouples).

Along the cylinder generatrix $\varphi = 0$ deg, there were 10 calorimetric heat flux sensors placed, with a minimum spacing of 8 mm. The sensors were made of brass disks, having a thickness of 0.15–0.25 mm and a diameter of 2 mm, and were thermally and electrically insulated from the model wall. The 0.1-mm chromel-copel thermocouples were welded to the inner surface of the disks. Near the solder point, these thermocouples were also rolled off to a thickness of 0.03–0.04 mm.

Both the thin wall and the calorimetric sensors required a calibration that was performed in a special impulse heat facility. Great care was taken in the processing of heat transfer measurements and the sources of errors, especially those due to lateral conduction, were evaluated. This careful analysis has shown that the error in the peak values did not exceed 5%. The effect of the wall thickness on the lateral heat diffusion was also small. These results confirm the small influence of lateral heat conduction on the data obtained in the present experimental investigation.

III. Effect of Shock Location and Shock Strength

A. Experimental Investigation

This part of the study was performed at Mach number $M_\infty = 6$ and Reynolds number $Re = 0.45 \times 10^6$. To vary the shock location and, hence, the flow pattern, the cylindrically blunted plate was moved vertically relative to the oblique shock generator. For example, at $\theta = 15$ deg, 13 different model configurations were tested. In the course of the experiments, each configuration was defined by two numbers: the horizontal and vertical distances between the plate and wedge (X and Y; Fig. 2). From a theoretical point of view, a more convenient characteristic of the configuration is the normalized distance between the cylinder and the point of intersection of the oblique shock with the x axis: x_*/r (Fig. 2).

The shock polar representation Γ_0 of the solution to the oblique shock equations is the locus of the states connected with the upstream state 0 by a shock wave. Its shape, for a constant value γ, depends only on the upstream Mach number M_0. In a plane of two variables, the pressure jump p_1/p_2 across the shock is plotted vs the direction σ of the velocity. The polar Γ_1, relative to the locus of the states connected with the state 1 by a shock wave, intersects the strong-shock branch of Γ_0 because of downstream conditions, which force the strong-shock solution for C_2 (Fig. 3b). The shock C_3 causes a transition from state 1 to state 3 such that the image of state 3 is situated at the intersection of the polars Γ_0 and Γ_1. Downstream of the two weak oblique shocks C_1 and C_3, the flow 3 is still supersonic, whereas state 2 is subsonic. Therefore, a strong discontinuity in velocity exists on either side of the slip line Σ_1 separating the flows 2 and 3 and stemming from the triple point I_1. In the type III interference, an attached shock C_4 is possible. What characterizes the type IV interference is the impossibility for the slip line to reattach at the wall. It follows a supersonic jet, as shown in Fig. 4. The polar representation in this case is the same as for type III interference. In both situations, the impact of the shear layer (type III) or of the supersonic jet (type IV) produces a steep rise in pressure and heat fluxes at the wall, as is shown by the present experiments.

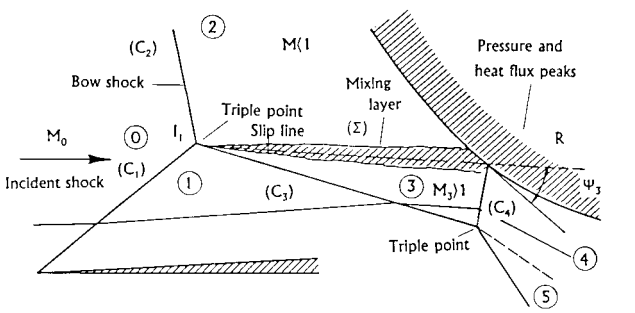

a) Physical plane

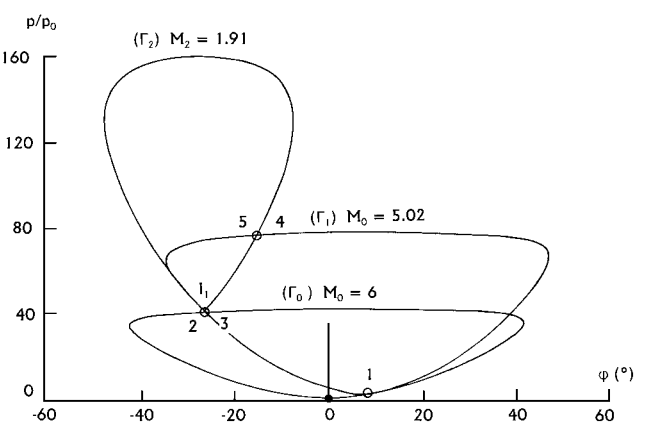

b) Hodograph plane ($M_0 = 6$)

Fig. 3 Type III interference.

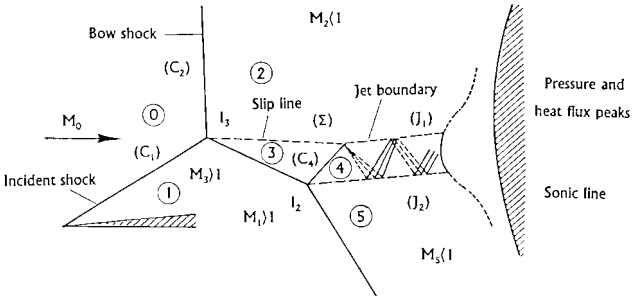

Fig. 4 Type IV interference.

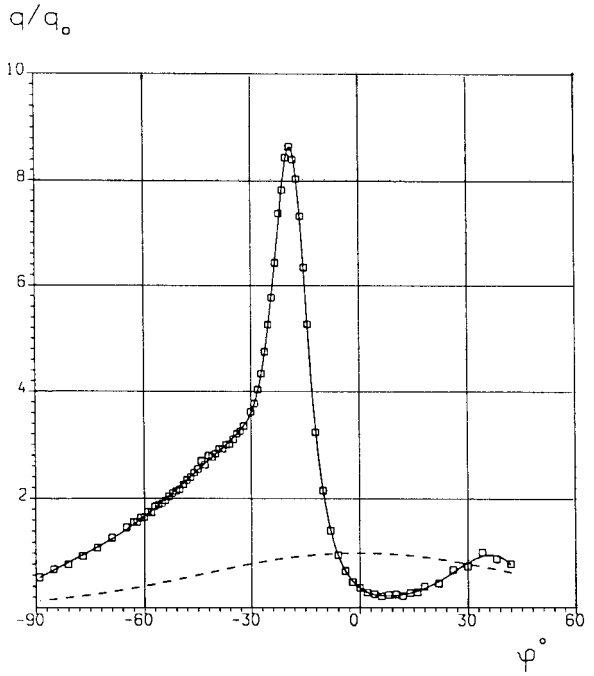

a) Heat transfer distribution on the cylinder

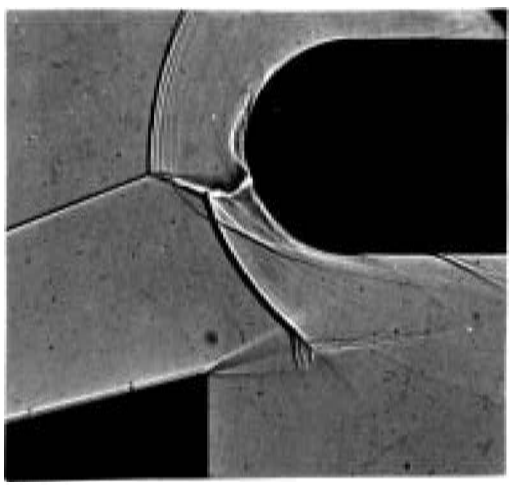

b) Shadowgraph of flowfield

Fig. 5 Type IV interference: $M_\infty = 6$, $Re = 0.45 \times 10^6$, and $\theta = 15$ deg, incident shock location; $x_*/r = -0.23$ ($X = 5$ mm and $Y = 17$ mm).

Heat transfer distributions and shadowgraphs for typical interference patterns at different shock positions ($\theta = 15$ deg) are presented in Figs. 5 and 6. The measured heat transfer rates are divided by the stagnation line heat transfer measured on the cylinder alone under the same conditions.

At a remote position of the impinging shock relative to the cylinder, the type IVa interference occurs. This case is characterized by a strong deflection of the high-pressure jet issued from the shear layer

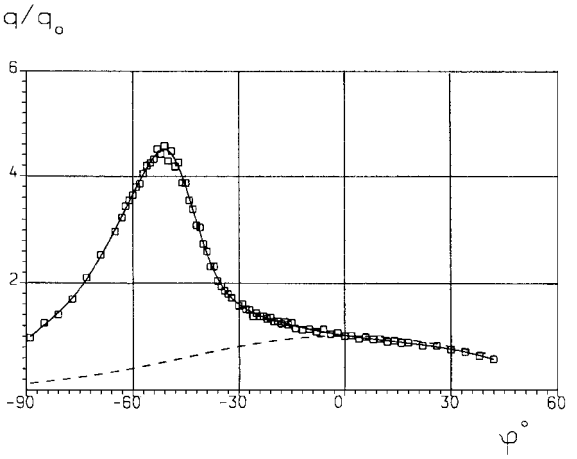

a) Heat transfer distribution on the cylinder

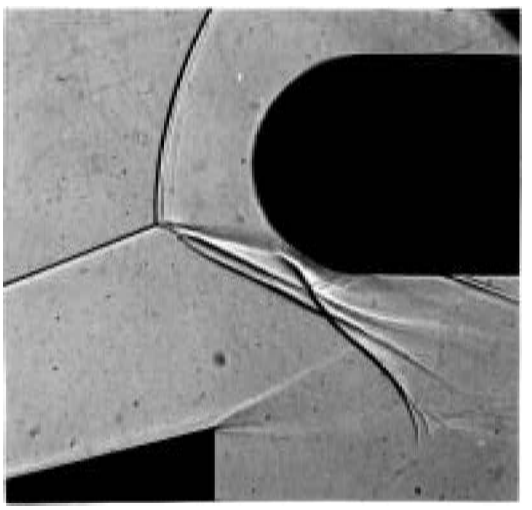

b) Shadowgraph of flowfield

Fig. 6 Type III interference: $M_\infty = 6$, $Re = 0.45 \times 10^6$, and $\theta = 15$ deg, incident shock location; $x_*/r = 0.42$ ($X = 5$ mm and $Y = 21.5$ mm).

emanating from the meeting point of the bow shock and the incident shock. This shock embedded within the subsonic shock layer is deflected upward and grazes the cylinder surface. Nevertheless, the heat transfer increases significantly (up to 4.6 times) near the grazing point. Apparently, this increase is due not only to the pressure increase but also to the jet turbulence.

The heat transfer achieves a maximum value for a type IV interference, when the high dynamic pressure jet impinges nearly normally on the cylinder surface (Fig. 5); the heat flux peak is located at the jet stagnation point (at $\varphi \approx -20$ deg). A second, smaller peak can be detected at $\varphi \approx 36$ deg. Shadowgraph analysis shows that this peak is due to the formation of a barrellike structure, i.e., high-pressure jet expansions and recurrent compressions. At the end of the barrel region, the pressure increases, which leads to an increase of heat exchange. As the distance x_* decreases, the high-pressure jet and the heat flux peak move downward. When $x_*/r > -0.02$, a type III interference is formed (Fig. 6a), where the shear layer coming from the shock triple intersection point hits the cylinder surface and an oblique shock is created by the deflection of the supersonic flow. The details of this flow are shown in Fig. 6a.

Normalized peak values of the heat flux are plotted as a function of x_*/r in Fig. 7. These values characterize the location of the impinging shock relative to the cylinder. Two maxima are clearly seen, with the second maximum at $x_*/r \approx 0$ exceeding the first one. In Fig. 8 the experimental results are presented in the form suggested by Wieting and Holden[3]: the heat flux peaks are plotted vs the angular coordinate φ_m at which the peak is reached. The first maximum is observed at $\varphi_m \approx -17$ deg, which is close to the result of Wieting and Holden[3] ($\varphi_m \approx -20$ deg). The second maximum is located much farther from the stagnation line (at $\varphi_m \approx -40$ deg).

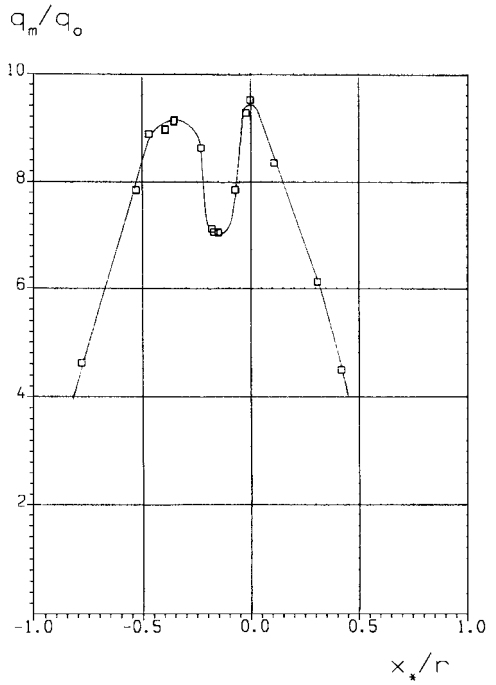

Fig. 7 Influence of shock location on the peak heat flux: $M_\infty = 6$, $Re = 0.45 \times 10^6$, and $\theta = 15$ deg.

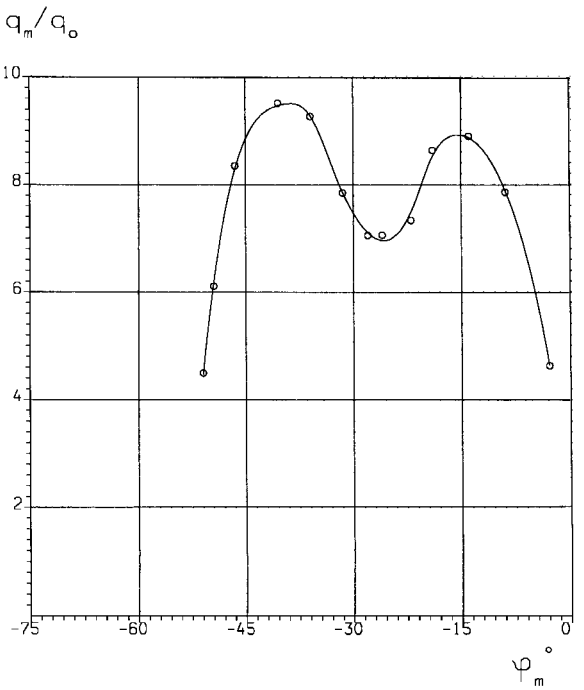

Fig. 8 Peak heat flux amplification vs peak angular location: $M_\infty = 6$, $Re = 0.45 \times 10^6$, and $\theta = 15$ deg.

To examine the effect of shock strength, two additional wedge angles, $\theta = 10$ and 20 deg, were investigated in detail, and experiments were also conducted for intermediate angles $\theta = 12.5$ and 17.5 deg. In the investigated range of wedge angles, no qualitative change in heat transfer was observed. Of the three angles investigated in detail ($\theta = 10$, 15, and 20 deg), the maximum heat flux was recorded for $\theta = 15$ deg. Some experiments indicate that the heat flux is larger for $\theta = 17.5$ deg than for $\theta = 15$ deg. Further increase of the wedge angle up to 20 deg results in a decrease of the maximum heat flux. These results agree with approximate calculations of the maximum pressure for the type IV interference.[2]

B. Inviscid Flow Calculations

The goal of these computations was to gain a deeper understanding of the interference flow pattern and, particularly, of the nonmonotonic dependence of peak heat flux on the shock position relative to the cylinder as observed in experiments. Of course, the inviscid gas flow cannot accurately reflect the real gas flow, but it may offer some insight into important features of the real flow. Also, it is easier to detect shock waves and expansion waves when viscosity is ignored.

Two-dimensional inviscid flows were computed using the second-order time-marching Godunov method[9] to solve the Euler equations. The bow shock was treated as a movable discontinuity across which the Rankine–Hugoniot equations could be applied. This shock-fitting method results in higher accuracy, especially at the triple points, than the capturing method. All interior discontinuities, such as contact lines, shock waves, expansion fans, and jets were captured, these discontinuities being smeared over several cells. The computational grid contained about 16,000 points. The second-order accuracy of the Godunov scheme was retained throughout, using Kolgan's corrections.[10]

The computations were performed for a perfect gas with a constant specific heat ratio $\gamma = 1.4$ at Mach number $M_\infty = 6$. The impinging shock was generated by a wedge of angle $\theta = 15$ deg. There were 13 shock positions (from $x_*/r = -1.36$ to 0.35) chosen (all dimensions were normalized by the cylinder radius). Three streamlines were calculated: the zero streamline stagnating on the cylinder surface and two streamlines emanating from the triple points (the zero streamline is marked by crosses in Figs. 9 and 10). These streamlines help to interpret the results. Figures 9 and 10 show the flow patterns based on the corresponding results.

Flow patterns for $x_*/r = -0.285$ and -0.395 should be referred to the type IV interference. However, there is an important difference between the flow patterns in Figs. 9 and 10: for $x_*/r = -0.285$, the zero streamline crosses the two oblique shocks AB and BD and a normal shock DE, whereas for $x_*/r = -0.395$, the zero streamline, in addition, goes through an expansion fan CE. The expansion results in an increase of total pressure losses and a decrease of stagnation pressure at point S. The possibility of an expansion fan forming depends on the normalized length of the jet (length of the jet between B and E divided by the jet width). At $x_*/r = -0.395$, the jet is long enough to include an expansion fan. Thus, the computations show that the maximum surface pressure can increase, when a type IV interference turns into a type III interference, because of a change in the wave structure in the jet. Consequently, the second heat flux maximum can be formed without laminar–turbulent transition.

The results presented in Fig. 11 show that a prediction based on an inviscid flow calculation and on the stagnation line boundary-layer

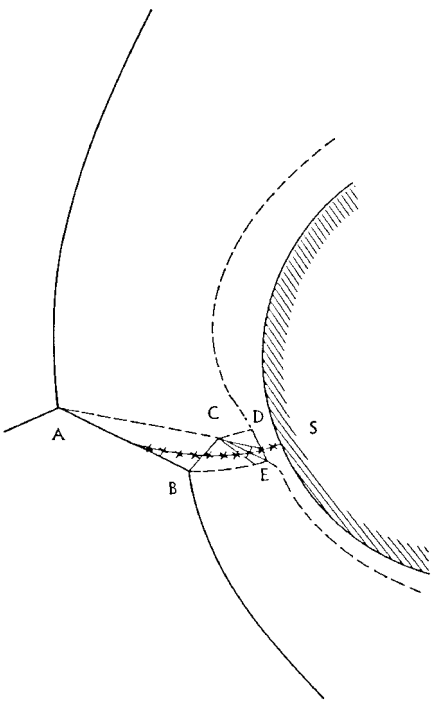

Fig. 9 Flow pattern for impinging shock location $x_*/r = 0.395$: type IV interference; $M_\infty = 6$ and $\theta = 15$ deg.

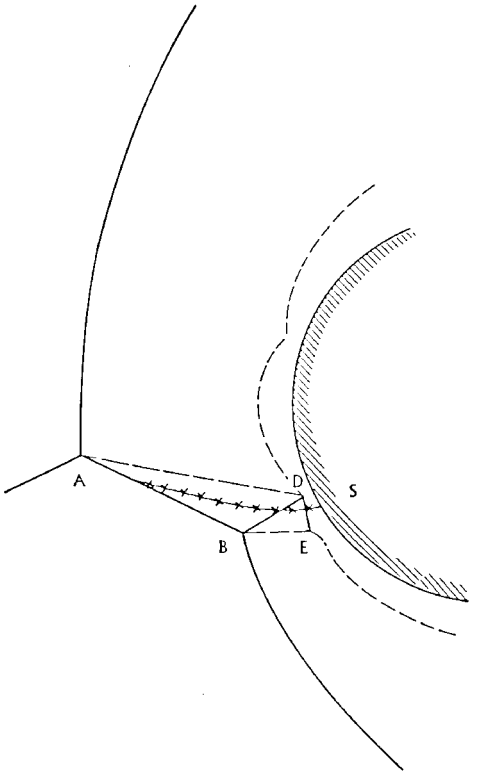

Fig. 10 Flow pattern for impinging shock location $x_*/r = -0.285$: type IV interference; $M_\infty = 6$ and $\theta = 15$ deg.

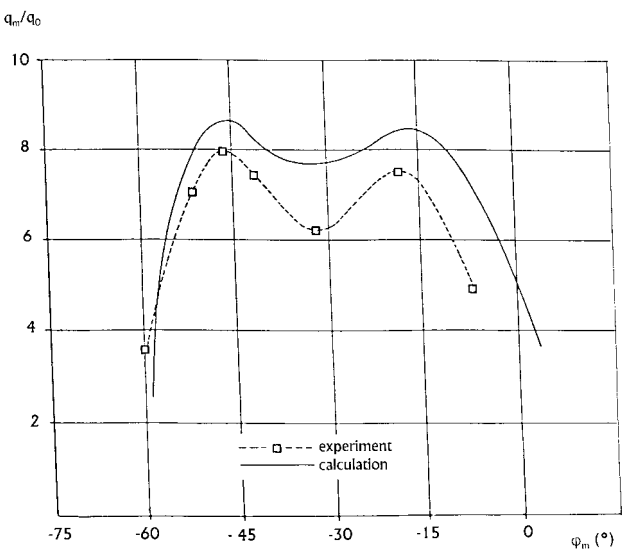

Fig. 11 Comparison of calculated and experimental heat transfer rate amplification: $M_\infty = 6$, $Re = 1.6 \times 10^6$, and $\theta = 15$ deg.

approach provides an adequate description of the relation between the peak heat transfer and the incident shock location. This simplified approach can be used for an approximate estimation of the peak heat values.

IV. Mach Number Effect

From an analysis of a large number of experimental results, it can be concluded that the difference between wave detachments above the incident shock, l_1, and below it, l_2, is significantly greater at $M_\infty = 16$ than at $M_\infty = 6$. This is due to the higher pressure difference in shock layers located below and above the incident oblique shock. However, the length of the transmitted shock is smaller at $M_\infty = 16$ than at $M_\infty = 6$ because its inclination angle with respect to the undisturbed flow direction at $M_\infty = 16$ is much smaller than at $M_\infty = 6$. The value of this angle depends on the pressure ratios across the normal shock and the incident oblique shock.

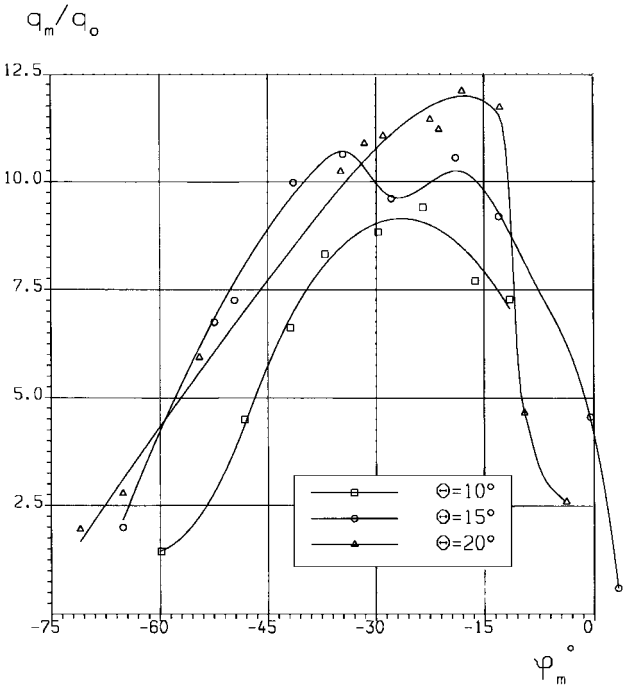

Fig. 12 Effect of impinging shock strength on peak heat flux amplification and location: $M_\infty = 16$ and $Re = 1.1 \times 10^4$.

Calculations, as well as experiments, show that this angle decreases with the Mach number.

The normalized maximum heat fluxes at $M_\infty = 16$ are presented in Fig. 12 as a function of the angular coordinate φ_m of the peak. The wedge angle $\theta = 20$ deg produces a higher heat flux than the smaller angles $\theta = 10$ and 15 deg. As mentioned earlier, at $M_\infty = 6$ the maximum heat flux was achieved for $\theta = 15$ deg.

At Mach numbers $M_\infty = 6$ and 16, the heat transfer peaks are located in the same region on the cylinder surface. For the wedge angle $\theta = 15$ deg, the function $q_m/q_0 = f(\varphi_m)$ has two maxima, at $M_\infty = 16$ and at $M_\infty = 6$, with the trough at $M_\infty = 16$ not as deep as at $M_\infty = 6$. For the wedge angle $\theta = 20$ deg, the trough at $M_\infty = 16$ is absent (Fig. 12). From Sec. III.B, it may be thought that the difference is a consequence of a change of the wave pattern in the high dynamic pressure jet. A peculiar feature of the function $q_m/q_0 = f(\varphi_m)$ at $\theta = 20$ deg is a sharp heat flux decrease when $\varphi_m \approx 10$ deg. Analysis of the schlieren pictures shows that this decrease related to the transition from a type IV flow to a type IVa flow, for which the high dynamic pressure jet only grazes the body surface.

The experiments show that the heat transfer amplification increases with Mach number. The maximum heat flux amplification at $M_\infty = 16$ is 12.

V. Reynolds Number Effect

In an interference flow, the Reynolds number can influence heat transfer to the cylinder front in two ways: 1) by displacement of the oblique shock/bow shock intersection point and 2) by modification of the interference flow due to change of the gas viscosity itself. The present study has shown that for Reynolds number (referenced on cylinder diameter) above 10^5, the normalized peak heat transfer depends weakly on Reynolds number. The peak heat flux is referred to the measured cylinder stagnation line heat flux, which is strongly influenced by acoustic disturbances generated by the nozzle boundary layer.[11] Thus, one can conclude that the acoustic disturbances, which arise at high Reynolds numbers, provoke a proportional increase of heat transfer, both in the interference flow and in the flow around the cylinder alone.

From Fig. 13, it is evident that two maxima are formed at the low Reynolds numbers $Re = 0.28 \times 10^5$ and 0.85×10^5, as well as at the high Reynolds number $Re = 0.45 \times 10^6$. Thus, the experiments show that the second heat flux maximum forms even at low Reynolds numbers. For $Re = 0.28 \times 10^5$, the estimated Reynolds

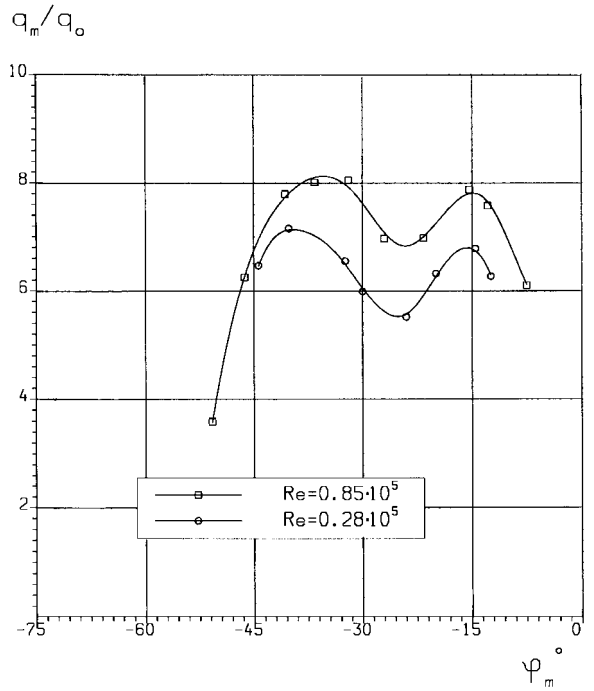

Fig. 13 Effect of Reynolds number on peak heat flux amplification and location: $M_\infty = 6$ and $\theta = 15$ deg.

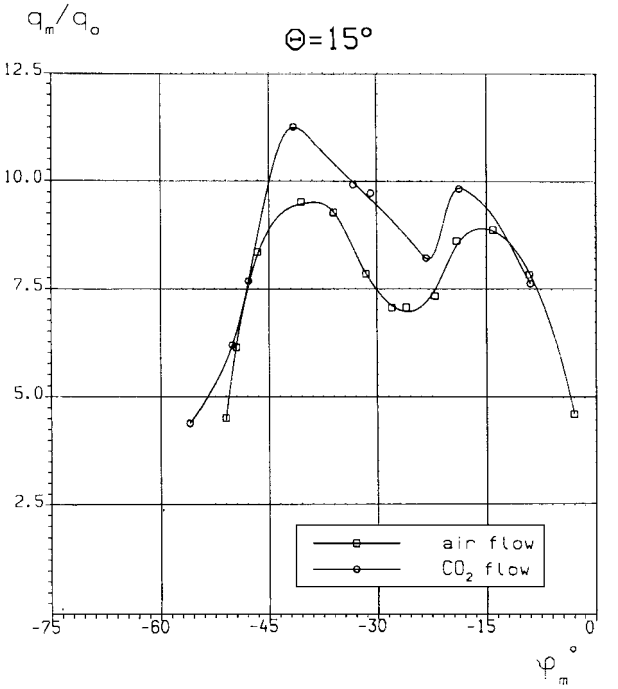

Fig. 14 Comparison of peak heat flux amplification/location in air and CO_2 flow. Airflow: $M_\infty = 6$, $Re = 0.45 \times 10^6$, and $\theta = 20$ deg. CO_2 flow: $M_\infty = 6.6$, $Re = 0.18 \times 10^6$, and $\theta = 20$ deg.

number based on the length of the shear layer is about 2.5×10^4, and the Reynolds number based on the length of the high-pressure jet is about 0.7×10^4. These values are lower than the critical value for laminar turbulent shear layer transition defined experimentally.[12] This confirms that the second heat flux maximum is not caused by the laminar–turbulent transition.

VI. Shock Wave Interference in Carbon Dioxide Flow

Experiments in carbon dioxide were undertaken to simulate the phenomena occurring in air flow at high temperature. Approximate calculations performed by Edney[2] for the type IV interference indicated significant amplification of the maximum surface pressure when the gas specific heat ratio is smaller. A reduction of γ should also lead to heat transfer amplification. Experiments in the CO_2 flow were performed for the following conditions: total pressure $P_0 = 38 \times 10^5$ Pa, total temperature $T_0 = 740$ K, Mach number $M_\infty = 6.6$, Reynolds number $Re = 0.18 \times 10^6$. The parameters chosen provide substantial variations of the gas state and specific heat ratio. On the other hand, Mach and Reynolds numbers in the CO_2 flow are close to similar values in the airflow.

Tests were carried out with the cylinder without impinging shock to determine the effective value of γ. This value was obtained by comparing the shock wave shape and detachment distance determined from shadowgraphs and from calculations. Good agreement was obtained with $\gamma_1 = 1.30$. Thus, the effective value of γ after the bow shock ($\gamma_{ef} = 1.30$) lies between the equilibrium value ($\gamma_{eq} = 1.202$) and the perfect two-atomic gas value ($\gamma = 1.400$) and differs significantly from both values. This means that in the CO_2 flow the main part of the shock layer behind the bow shock was in nonequilibrium.

Although interferences in CO_2 and in air are similar, shadowgraphs and heat flux measurements reveal a strong quantitative influence of the specific heat ratio. In both cases, the detachment of the oblique shock from the wedge, as well as the detachment of the bow shock from the cylinder, are essentially less in CO_2 than in the air. This is because a greater part of the energy in a CO_2 flow is transformed into the internal degrees of freedom; hence, the specific heat ratio γ is less than in an airflow. Thus, the oblique shock/bow shock intersection point in CO_2 is located closer to the wedge surface than in air.

With the first configuration, a type IV interference forms in the airflow, whereas a type III occurs in the CO_2 flow. In spite of this, the peak heat flux amplification in CO_2 ($q_m/q_0 = 11.2$) is higher than in air ($q_m/q_0 = 8.6$). This can be explained by an increased compression degree in the CO_2 flow due to a lower γ. With the second configuration, a type III interference takes place both in air and CO_2. However, in CO_2 the shear layer runs significantly lower and encounters the cylinder surface at a smaller angle than in air. In this case, the peak heat flux amplification in CO_2 ($q_m/q_0 = 4.4$) is less than in air ($q_m/q_0 = 6.1$).

The maximum values in CO_2 and in air are very different for the same value of wedge angles ($\theta = 20$ deg in Fig. 14): the maximum heat flux normalized value in CO_2 is two times higher than in air. In CO_2, the function $q_m/q_0 = f(\varphi_m)$ has two maxima, as in air. The second maximum is attained at $\varphi_m \approx -40$ deg, when the type IV interference turns into a type III. It is higher than the first maximum at $\varphi_m \approx -20$ deg.

VII. Conclusions

1) An extensive experimental investigation of heat transfer on the cylinder front surface for the types III and IV interference has been performed, and a large quantity of data has been collected under different conditions (Mach and Reynolds numbers, shock strength and location, specific heat ratio) constituting a well-documented database for validation of computation methods.

2) In the interference region, the normalized heat transfer rate depends weakly on the Reynolds number, when it is greater than 10^5. This means that the acoustic disturbances that arise at high Reynolds number cause a proportional increase of heat transfer both in the interference flow and in the flow around the cylinder alone.

3) A nonmonotonic variation of the peak heat transfer level with the peak position was found. Two maxima were observed: one at $M_\infty = 6$ on the cylinder generatrix $\varphi_m \approx 20$ deg when a type IV interference occurs and a higher maximum at $\varphi_m \approx 40$ deg when the type IV becomes type III. Analysis of numerical and experimental data shows that the second peak is due to a change in the flow pattern of the high dynamic pressure jet, in particular to the disappearance of an expansion fan in this jet.

4) The decrease of the specific heat ratio in the CO_2 flow changes the flow pattern and heat transfer in the interference region significantly. The maximum heat transfer amplification is higher in CO_2 than in air, in agreement with the theoretical results of Edney[2] and other investigators.

Acknowledgments

This study was performed with the financial support of the Direction de la Recherche et de la Technologie of the French Ministry of Defense. The authors are grateful to V. Ya. Bezmenov, S. M. Boldyrev, I. F. Chelysheva, B. V. Egorov, S. N. Krutiy and L. V. Yakovleva for their very valuable help in performing this investigation.

References

[1]Teterin, M. P., "Investigation of a Supersonic Gas Flow and Heat Transfer in the Region of an Incident Shock Wave on a Cylinder," *Izvestia AN SSSR (Scientific Messages of the USSR Academy of Sciences), Mechanica Zhidkosti i Gasa (Fluid Mechanics Journal)*, No. 2, 1967, pp. 143–147, and No. 3, 1967, pp. 92–97; also NASA TT F-11, 795, 1968.

[2]Edney, B., "Anomalous Heat Transfer and Pressure Distributions on Blunt Bodies at Hypersonic Speeds in the Presence of an Impinging Shock," Aeronautical Research Inst. of Sweden, FFA Rept. 115, 1968.

[3]Wieting, A. R., and Holden, M. S., "Experimental Shock-Wave Interference Heating on a Cylinder at Mach 6 and 8," *AIAA Journal*, Vol. 27, No. 11, 1989, pp. 1557–1565.

[4]Holden, M., and Kolly, J., "Measurements of Heating in Regions of Shock/Shock Interaction in Hypersonic Flow," AIAA Paper 95-0640, Jan. 1995.

[5]Mohamed, A. K., Pot, T., and Chanetz, B., "Diagnostics by Electron Beam Fluorescence in Hypersonics," 16th International Congress on Instrumentation in Aerospace Simulation Facilities, Dayton, OH, July 1995.

[6]Prabhu, R. K., Stewart, J. R., and Thareja, R. R., "Shock Interference Studies on a Circular Cylinder at Mach 16," AIAA Paper 90-0606, Jan. 1990.

[7]Gaitonde, D., and Shang, J. S., "On the Structure of an Unsteady Type IV Interaction at Mach 8," *Computers and Fluids*, Vol. 24, No. 4, 1995, pp. 469–485.

[8]Darracq, D., and Gazaix, M., "Computation of Viscous Shock/Shock Interaction with an Upwind LU Implicit Scheme," 19th International Symposium on Shock Waves at Marseille. Pt. 4 (Université de Provence, Marseille, France), Springer, 1995.

[9]Godunov, S. K., Zabrodin, A. B., Ivanov, M. Y., Krayko, A. N., and Prokopov, G. P., "Numerical Solution of Multi-Dimensional Gas Dynamics Problems," *Nauka*, 400, 1976.

[10]Kolgan, V. P., "Use of the Principle of Derivative Minimum Value for a Design of Finite-Difference Schemes When Solving Gas Dynamic Equations with Discontinuities," *Uchenye Zapiski TsAGI*, Vol. 3, No. 6, 1972, pp. 68–77.

[11]Borovoi, V. Y., Chilinov, A. Y., Gusev, V. N., Struminskaya, I. V., Délery, J., and Chanetz, B., "Interference Between a Cylindrical Bow Shock and a Plane Oblique Shock," AIAA Paper 96-2046, June 1996.

[12]Birch, S. F., and Keyes, J. W., "Transition in Compressible Free Shear Layers," *Journal of Spacecraft and Rockets*, Vol. 9, No. 8, 1972, pp. 623, 624.

P. R. Bandyopadhyay
Associate Editor